Hindawi
Structural Control and Health Monitoring
Volume 2023, Article ID 1552150, 22 pages
https://doi.org/10.1155/2023/1552150

Research Article

Seismic Mitigation Effect of Lever-Type Lead Viscoelastic Node Dampers

Mao Ye,[1] Jin Jiang,[2] Jingya Zhou,[1] Wuliang Zhang,[1] Baotao Huang,[3] and Ming Wu[2]

[1]*Wind Engineering and Engineering Vibration Research Centre, Guangzhou University, Guangzhou 510006, China*
[2]*Department of Civil and Intelligent Construction Engineering, Shantou University, Shantou 515062, China*
[3]*School of Marine Engineering Equipment, Zhejiang Ocean University, Zhoushan 316022, China*

Correspondence should be addressed to Jin Jiang; jian0048@e.ntu.edu.sg

Received 24 April 2023; Revised 15 September 2023; Accepted 7 October 2023; Published 13 October 2023

Academic Editor: Lin Chen

Energy dissipation damping technology is usually used for infrastructure construction in seismic regions. In this study, a lever-type lead viscoelastic node damper (LTLVND), which can capture small rotational displacements of the infrastructure under seismic excitation, is innovatively proposed based on the leverage effect. The characteristics of energy-absorbing capacity of the LTLVND and its mitigation effect on the dynamics of the structure under seismic excitation are studied. Testing and modelling results show that a satisfactory energy dissipation effect can be observed for the innovative lead viscoelastic damper (LTLVND). Finally, a seismic analysis of a concrete frame structure with LTLVNDs is carried out. Pushover analysis and dynamic elastoplastic analysis are included. It is shown that a significant improvement in structural performance under seismic conditions can be achieved with the addition of LTLVNDs at appropriate locations.

1. Introduction

The installation of energy-dissipating structural members and passive damping systems are two widely accepted solutions for reducing vibration in building structures. However, the disadvantages of energy-dissipating structural members, including severe plastic deformation and failure under severe seismic excitation, make them inappropriate in some cases. Incorporating structural dampers into a structure can improve its dynamic performance by absorbing a substantial amount of vibrational energy. Therefore, passive energy dissipation systems such as base isolation technology and structural dampers are commonly used to improve the dynamic response of infrastructure in new design or retrofit scenarios. Today, types of structural dampers including metallic dampers made of mild steels, deformable memory alloys, or lead, friction dampers, viscoelastic dampers, and viscous dampers are well developed and applied as energy dissipation devices [1–6]. Viscoelastic dampers are among the earliest types of passive dampers and are well applied in a number of infrastructures to minimize motion amplitude and acceleration as a result of wind or seismic excitation.

Metal dampers are capable of reducing the structural movement under dynamic loading when properly applied. The feasibility of using metal dampers to mitigate a structural response under seismic attacks has been widely investigated [7, 8]. Friction dampers, which have the advantage of good energy dissipation capacity, have also been successfully used to dissipate energy through the relative displacement between internal friction plates and the bolt. However, material degradation and permanent misalignment could be produced on contact surfaces under cyclic force, and good maintenance should be given to these contact surfaces. Hydraulic devices are used as viscous dampers to dissipate the kinetic energy of seismic events and to cushion the impact between structures. Roy and Matsagar [9] studied the effectiveness of passive vibration control devices used to retrofit multistory steel buildings under dynamic forces. Pant et al. [10] studied the performance of viscoelastic coupling dampers based on full-scale tests and to assess the suitability of different numerical models in

predicting their response. Rahimiasl and Bakhshi [11], Kinali and Ellingwood [12], and Lignos and Karamanci [13] carried out seismic fragility assessments of frame structures for consequence-based engineering. Choi et al. [14] investigated smart dampers using a combination of magnetic friction and precompressed rubber springs. Gandelli et al. [15] studied the effect of acceleration-sensitive nonstructural components on hysteretic behaviour.

The interstory displacement is normally used to evaluate the energy dissipation capacity of dampers. The relative deformation of the beam-column joint can also be used for energy dissipation, especially for precast concrete structures. Iyama et al. [16] and Rojas et al. [17] studied the seismic performance of a friction device for posttensioned steel beam-column joints for moment resisting frames. Morgen and Kurama [18] and Eldin et al. [19] suggested a few friction dampers for the beam-column joints used in seismic building applications and existing reinforced concrete structures. Wang et al. [20] investigated the mechanical behaviour of superelastic SMA angles as seismic self-centering devices. Dehghani et al. [21] studied the seismic performance of a curved damper for a semirigid moment frame. Fang et al. [22] proposed an SMA ring spring system for beam-to-column self-centering connection. Dong et al. [23] studied the seismic performance for retrofitted RC frames by adding haunched viscoelastic damping braces. All dampers mentioned in this section are installed at the beam-column joint.

Significant efforts have been made to improve the seismic performance by enhancing the deformation capacity of the damper. Constantinou et al. [24] suggested a toggle-brace-damper seismic energy dissipation system to amplify the effect of damping devices. Sigaher and Constantinou [25] suggested a scissor-jack-damper energy dissipation system, which is a variant of toggle-brace-damper systems. Hwang et al. [26] presented a rotational inertia damper combined with toggles, which work effectively even in structures with small displacements. The aforementioned damper response enhancement technique uses link mechanisms. Berton and Bolander [27] developed an amplification system for dampers using gear mechanisms. Ribakov and Reinhorn [28] and Zasso et al. [29] suggested some efficient dampers with a lever mechanism for response reduction in buildings under load. Recently, Hsu and Halim [30] proposed an effective steel-curved damper, which can significantly amplify story drift through the leverage mechanism. Mosquera et al. [31] proposed an amplification system for concentrated and distributed energy dissipation devices, which combined amplification mechanisms and one or more dampers. Zhang et al. [32] studied a novel deformation-amplified SMA-friction damper to control the seismic responses of buildings.

As mentioned above, the interstory drift is normally used to evaluate the energy dissipation effect. However, interstory dampers will take up more space and tend to affect the use and aesthetics of the building. Hence, arranging node dampers to provide energy dissipation capacity becomes an option to improve structural seismic performance, energy dissipation capacity, and structural collapse resistance [33–35]. By this way, the failure region of the structure can be shifted from the connection to the beam [36]. However, compared with the interstory displacement, the relative deformation between beam-column nodes is smaller. It is more difficult for the node damper to produce energy dissipation.

To this end, a lever-type lead viscoelastic node damper (LTLVND) is proposed, which can capture small rotational displacements of the beam-column joint and effectively reduce the dynamic response under seismic excitation based on the leverage effect. It can also be installed in lieu of energy-dissipating structural members or heavy space occupying structural dampers.

2. Design Concept of Lever-Type Lead Viscoelastic Node Dampers (LTLVNDs)

To effectively dissipate the energy due to seismic excitation or other dynamic loads on the beam-column joints of the frame structure, a lever-type lead viscoelastic node damper (LTLVND) is proposed based on the idea that the arc length is proportional to the radii of a fan-shaped damper when the rotation centre is given. Figure 1 shows the design concept of the LTLVND, in which displacement amplification can be achieved by the leverage effect. When an angular deformation between the beam and the column, a_0, is produced, the outer arc plate of the damper would have a displacement of $d = ra_0$. As a result of the leverage effect, the displacement of the outer arc of the shear plate will have the displacement of $D = dR/r$ and the small displacement generated on the structure can be amplified according to the ratio of r to R.

Schematically, the LTLVND is composed of the skeleton panels (the inner panel and the outer panel), the shear plate, viscoelastic material, lead cylinders, and two rotating shafts (No. 1 and No. 2), as shown in Figure 2. A sliding sleeve hole is initially designed and prepared so that rotating shaft No. 2 can slide freely and no tensile force is generated in the shear panel. The rotary shear steel plate and the fixed steel plate are assembled, and the lead cylinders are then filled into the target slots. Rotating shaft No. 2 is used to fix the rotating shear steel plate and the fixed steel plate. When a displacement is given, the rotating shear steel plate would rotate along rotating shaft No. 1. The vulcanization effect under a high-temperature and pressure condition is applied to achieve the connection integrity of rubber and steel plates to prevent their separation during the energy dissipation process. The energy dissipation of the damper is mainly from the lead cylinder and viscoelastic material. Therefore, when a small displacement is produced in the structure under seismic action or wind load, the damper can hence effectively dissipate energy and reduce vibration to prevent plastic yielding or crack failure.

The LTLVND can be applied in beam-column joints of building structures as well as bridge structures with design purpose of energy dissipation. The space-saving LTLVND can capture the small displacement of the beam-column joint due to the amplification effect under seismic excitation and achieve the capability and functionality of energy

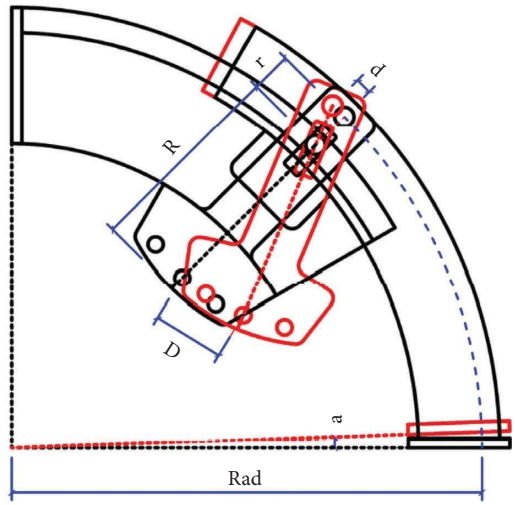

Figure 1: The design concept of LTLVNDs.

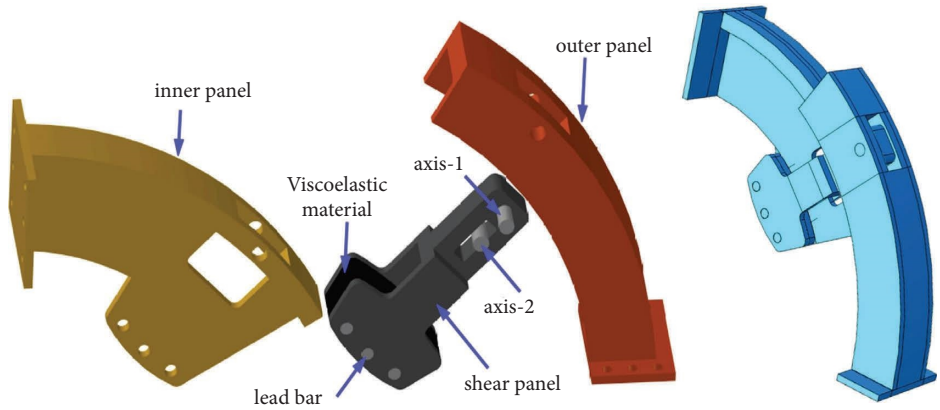

Figure 2: The components of LTLVNDs.

dissipation. Two energy-dissipating materials (lead and rubber) and two energy-dissipating actions (shear hysteresis and extrusion hysteresis) are included. In addition, the energy dissipation capacity of the LTLVND can be adjusted according to the leverage effect to meet the seismic mitigation and retrofit requirements for different seismic intensities. It has the advantage of accessibility of installation that the damper can be installed directly in the structure without additional supports to achieve the purpose of space saving.

The main innovation of this paper is to propose a lever-type lead viscoelastic node damper with deformation amplification capability. The LTLVND proposed in this paper can fully exert the energy dissipation effect in the case of small displacement of the structure and can effectively achieve the seismic mitigation effect. To a certain extent, the structure can be prevented from prematurely entering nonlinear deformation and failure. According to the lever principle, the small displacement generated by the structure can be amplified according to different rod-axis ratios. By amplifying the displacement or rotation angle of the structure, the energy dissipation capacity of the displacement damper can be fully utilized. In addition, the size of the LTLVND is small, and it can be installed at the beam-column joints of the building structure without affecting the use of the internal space of the building.

3. Experimental Investigation

3.1. Overview. To study the mechanical performance of LTLVNDs under cyclic loading, two specimens with the same geometric design are fabricated and tested to verify the capability and functionality of the energy dissipation capacity (Figure 3). One of the specimens is filled with lead cylinders in three reserved slots (LTLVND-1), while the other one is designed without lead filling in the slots (LTLVND-2). Figure 4 shows the testing specimen. To precisely obtain the design configuration of the LTLVND, the skeleton panel and the shear panel are first prepared according to the design size and configuration. The slots for lead cylinders and bolt connection are then prepared to the exact design location and size. The vulcanization step is then followed for the constrained steel plates and rubber layer under a high-temperature and high-pressure environment

to achieve good structural integrity of the damper. Finally, lead is poured into the reserved slots, and steel plates are used to seal the opening for NLDV-1.

3.2. Test Setup, Loading Scheme, and Observation. A precisely fabricated LTLVND was mounted at the L-shaped loading frame to examine energy dissipation performance as shown in Figure 5. The sinusoidal cyclic loading scheme was adopted, and the MTS servo actuator with a maximum loading capacity of 500 kN and a displacement of ±250 mm was used to produce a horizontal displacement (Figure 6). The schematic diagram of the L-shaped loading setup and the location of the linear variable differential transformers (LVDTs) are shown in Figure 7.

The sinusoidal cyclic load was applied at the end of the column of the L-shaped loading frame using a multifunctional electrohydraulic servo actuator mounted on the reaction wall. The load was initially applied at a frequency of 0.05 Hz and a displacement of ±1 mm for three cycles. The displacement was then sequentially increased to ±2 mm, ±4, ±6, ±8, and ±10 at each load level for three cycles. Note that the displacement control was used throughout the test. A calibration test was initially carried out to make sure the loading system and data acquisition systems were in good condition. The load applied at the top of the L-shaped frame drives the rotation of the pin connection, so the displacement at the top of the column can be converted to the displacement at the bottom of the frame. The data acquisition system, TDS-530, was used to monitor and record the real-time force and displacement. Figure 7 shows a schematic diagram of the LVDT distribution.

When a 2 mm displacement load was applied, a small but observable deformation occurred in the LTLVND could be found. When the displacement was increased to 4 mm, the dislocation between the shear panel and the skeleton panel occurred with a phenomenon that the paint was scraped off at the lower bolt connection, which means that a high shear force and shear deformation were produced between the LTLVND and the test frame. With an increase in the activator's displacement, the misalignment between the skeleton panel (inner panel and outer panel) and the shear panel became more severe. The deformation of the rubber due to the shear force between the skeleton panel and the shear panel increased accordingly. When the displacement of the activator was increased to 8 mm, the slip dislocation between the skeleton panel and the shear panel could be clearly observed.

3.3. Testing Result and Analysis. Figure 8 shows the hysteresis curves of LTLVNDs under cyclic loads. Figure 9 shows the skeleton curves of LTLVND-1 and LTLVND-2. The flattened distribution hysteresis loops can be found for LTLVND-2, which has no lead filling at three slots, while symmetrically oval-shaped hysteresis curves can be observed for LTLVND-1. This means that the energy dissipation capacity of LTLVNDs is significantly dependent on the presence of lead cylinders and rubber. As

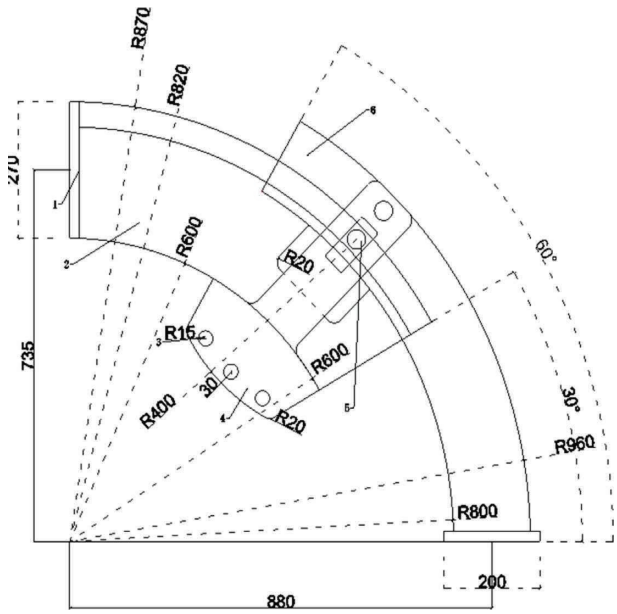

Figure 3: The geometrical details of LTLVNDs.

Figure 4: The testing specimen.

the displacement load gradually increases, the area of the hysteresis loops and energy dissipation capacities increase accordingly. As deformation increases, the damping force also increases. The pinching effect, which is a progressive deterioration of the structural stiffness under cyclic loading, can be observed. This phenomenon could be due to the reasons that (1) the lead cylinders filled in the slots would gradually shrink and the effective areas become smaller when a higher displacement load is applied and (2) a small gap exists between the rotation shaft and the skeleton panel. With regard to the effect of the lead cylinders, the energy dissipation of LTLVND-1 with lead filled in three slots is much higher than that of LTLVND-2. As a result of the gap between the rotating shaft and LTLVNDs, the energy dissipation capacity of LTLVNDs shows a thin hysteresis loop at the very beginning and an

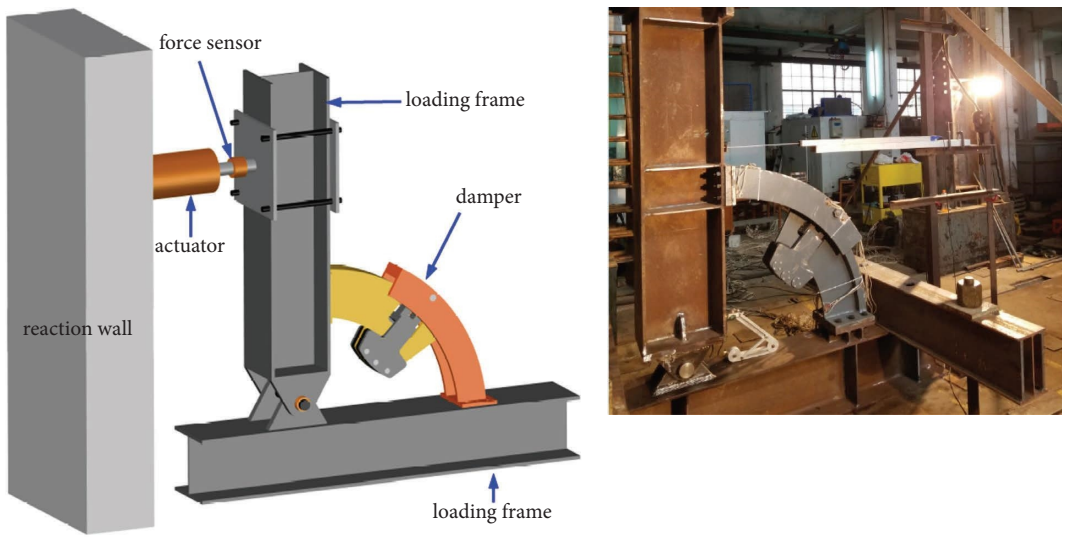

Figure 5: The test setup. (a) The schematic test setup. (b) Testing frame and LTLVND.

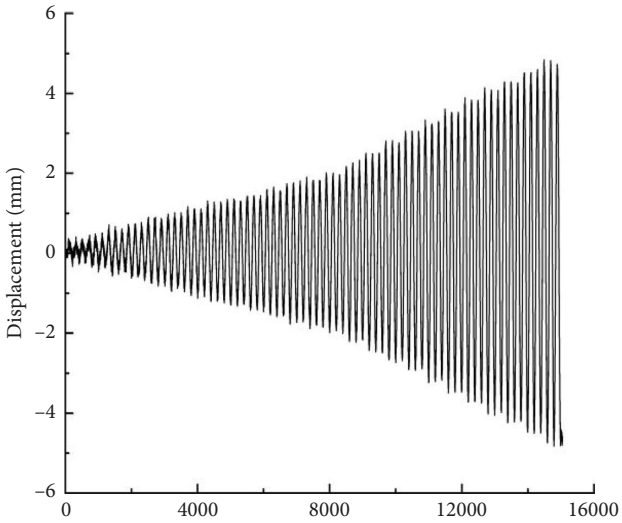

Figure 6: The applied cyclic loading.

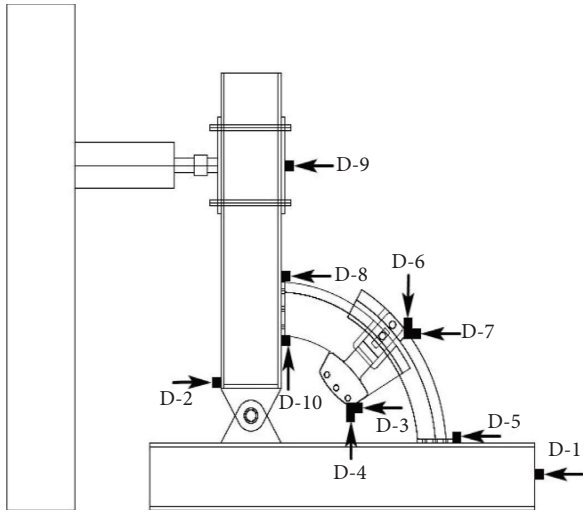

Figure 7: Location of LVDTs.

expanded hysteresis loop after yielding. It can be seen that lead and rubber in LTLVNDs work together to achieve energy dissipation by the shear effect.

Figure 10 shows the stiffness degradation of LTLVND-1 and LTLVND-2. It can be seen that the structural stiffness of LTLVND-1 is higher than that of LTLVND-2. At the early loading stage, the stiffness degradation rate of LTLVND-2 is slower than that of LTLVND-1. However, it increases at a higher degradation rate when the displacement reaches 6 mm for specimen LTLVND-2. For LTLVND-1, the stiffness degradation rate has minor changes throughout the loading process. Figure 11 shows the cumulative energy dissipated for LTLVND-1 and LTLVND-2.

4. Benchmark FE Modelling and Parametric Study

4.1. Model Development. In this study, general-purpose finite element modelling package ABAQUS [37] is used to model the performance of LTLVNDs under cyclic loads. A general-purpose linear brick element with reduced integration C3D8R is selected for the FEM analysis (Figure 12). For the constitutive model of steel Q235, a bilinear kinematic model with the Bauschinger effect is applied as shown in Figure 12. Note that there is no stiffness degradation under cyclic loading. Lead is regarded as an ideal elastoplastic material with yield stress f_y of 10.5 MPa, elastic modulus E of 16.46 GPa, and Poisson's ratio ν of 0.42.

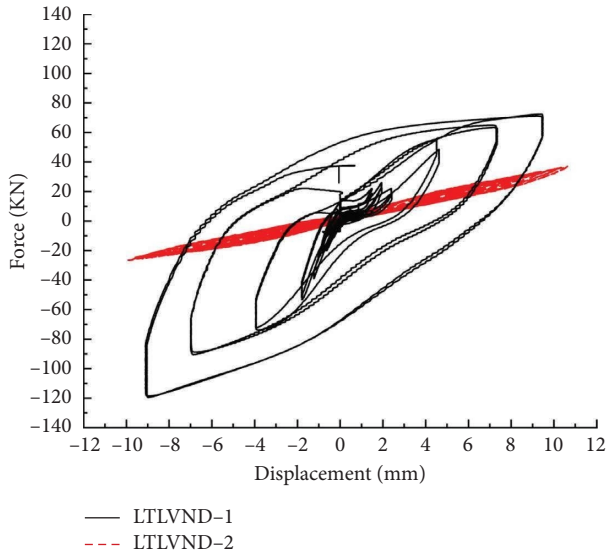

Figure 8: The hysteresis curves of LTLVNDs under cyclic loads.

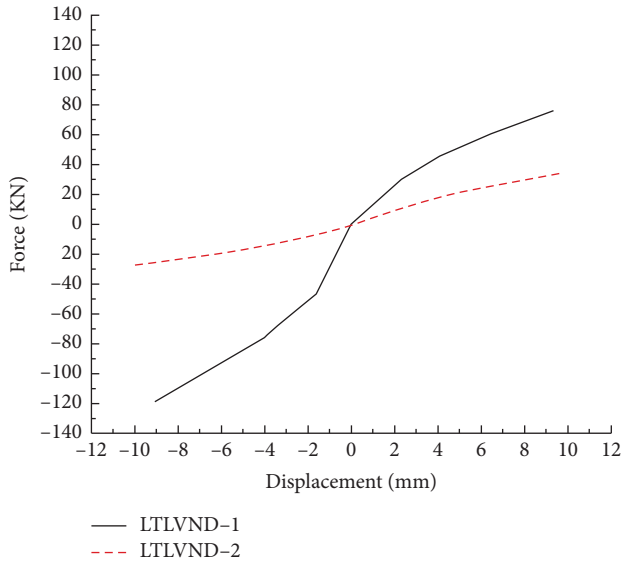

Figure 9: The skeleton curves of LTLVNDs.

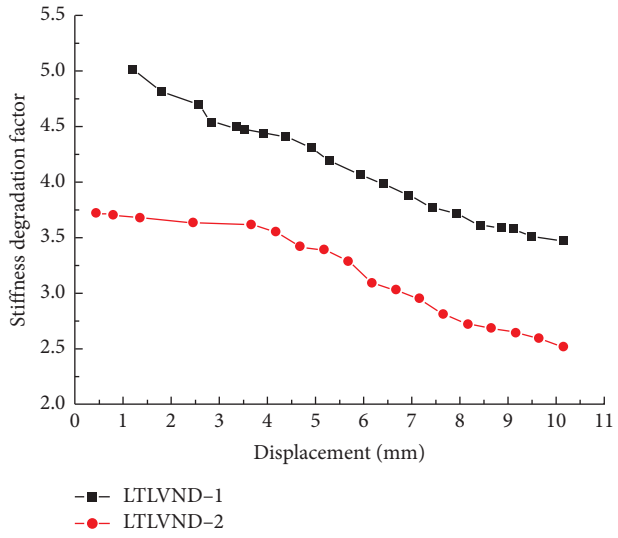

Figure 10: The stiffness degradation curve.

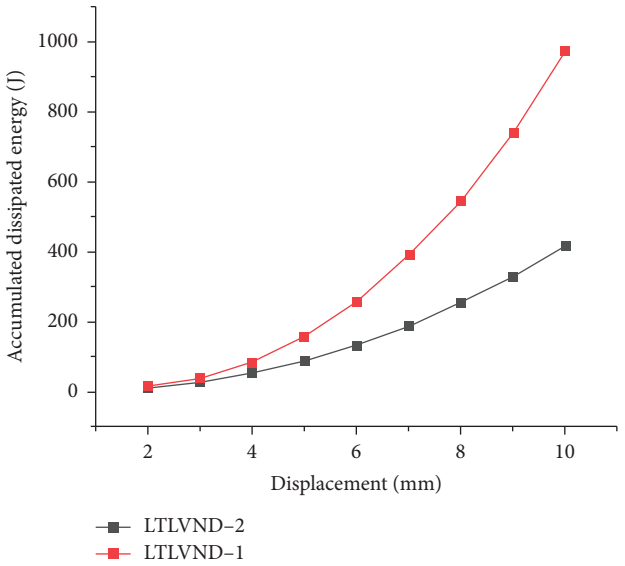

Figure 11: Cumulative dissipated energy.

Rubber is modelled as a hyperelasticity polymer material with characteristics of nonlinear large strain and volume incompressibility. Two popular constitutive models for rubber are commonly used: one is based on continuum mechanics and the other one is based on statistical mechanics theory. In this paper, the Mooney–Rivlin model based on continuum mechanics theory in which the mechanical strain energy is expressed as the sum of invariants is used to model the mechanical behaviour of rubber. The constitutive model for rubber was determined through fitting tests, and comparative analyses were conducted in ABAQUS using various rubber constitutive models, such as the Mooney–Rivlin model, polynomial model, neo–Hookean model, and Yeoh model, to develop a finite element model for LTLVNDs. Upon comparing these models with experimental data, it was found that the Mooney–Rivlin model provided a better representation of LTLVND's behaviour. As a result, the Mooney–Rivlin model was chosen for the analysis. The total strain energy can be expressed as equation (1). Table 1 shows all the input parameters for the Mooney–Rivlin model:

$$W = \sum_{i+j=1}^{N} C_{ij}\left(I_1 - 3\right)^i \left(I_2 - 3\right)^j + \sum_{k=1}^{N} \frac{1}{D_k}\left(I_3^2 - 1\right)^{2k}, \quad (1)$$

where W is the strain energy, C_{ij} and D_k are constants of the material, and I_1, I_2, and I_3 represent invariants with the deformation tensor of rubber.

The material properties of lead are crucial factors influencing the energy dissipation capacity of LTLVNDs. As lead is an ideal elastic-plastic material, the elastic modulus and yield strength of lead are the two most critical

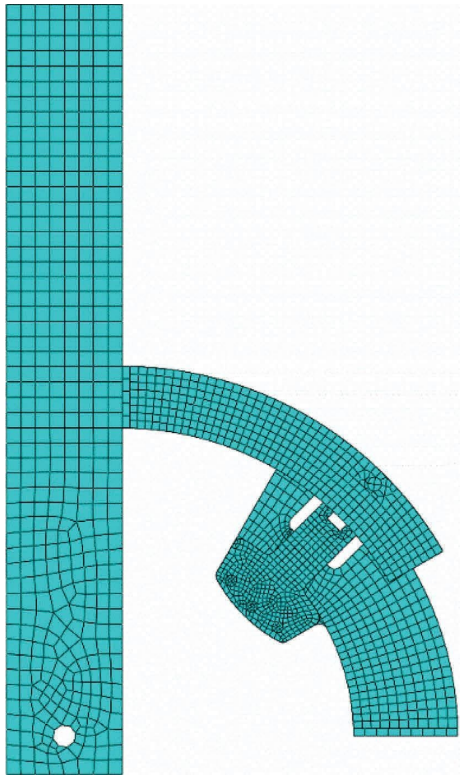

Figure 12: The mesh of LTLVNDs.

Table 1: The inputted parameters for the Mooney–Rivlin model (unit: MPa).

C_{10}	C_{01}	C_{20}	C_{30}	C_{11}
0.20601	0.0018577	0.0041001	0.0010092	2.807×10^{-5}

$G = E/3 = 2(C_{10} + C_{01}) = 0.4$ MPa and $C_{01}/C_{10} = 0.05$.

parameters affecting the energy dissipation capacity of LTLVNDs. Similar to the test setting, cyclic displacement control loading is applied to study the cyclic behaviour of the LTLVND. An incremental displacement is used to achieve the maximum deformation capacity of the model used. Figure 13 shows the constitutive models for the materials used in the modelling process.

4.2. Modelling Validation. Figures 14 and 15 show a comparison of the hysteresis curves and the skeleton curves from test and modelling, respectively. An obvious difference between the test results and the modelling results can be observed when a small displacement (±2 mm) is given. This phenomenon may be due to the gap and the sliding effect caused by the gap between the rotating shaft and the skeleton panel. The bilinear model of the restoring force is obtained, and the equivalent stiffness difference between modelling and testing is less than 10%. Hence, a good and reasonable agreement of the hysteresis curve can be observed.

There are several reasons that can lead to analysis errors between modelling and testing. First, the damper proposed in this paper requires a deformation

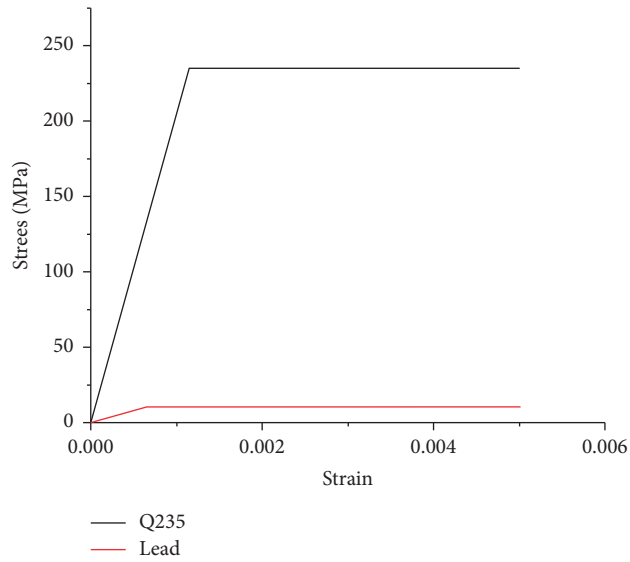

Figure 13: The constitutive models for materials.

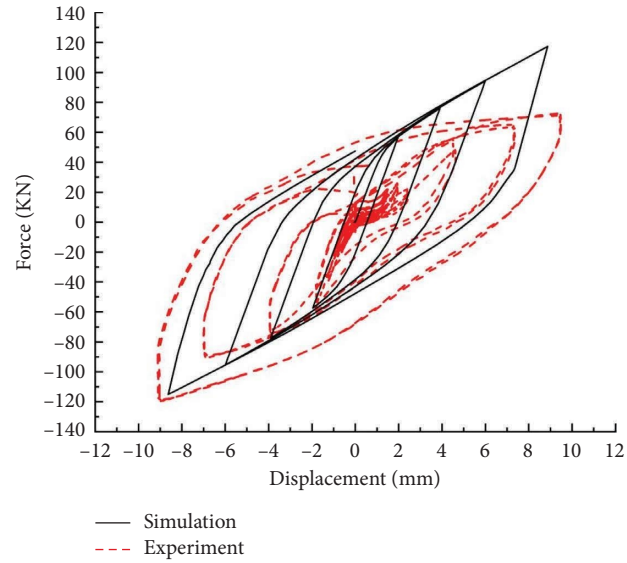

Figure 14: Comparison of the hysteresis curves from test and modelling results.

amplification function, and its details are more complicated than those of popular dampers. There are two rotating shafts (axis-1 and axis-2) in the damper. This relatively complicated structure could lead to insufficient precision in machining. Second, the connection between the reaction frame and the "L"-shaped loading frame also has a machining precision problem. Third, due to the precision of the loading scenario and the design of the joint, the actual loading condition might not match the preset loading condition. The accumulation of these factors caused significant numerical result errors. On the whole, a reasonable agreement of the hysteresis curve between modelling and testing can be observed.

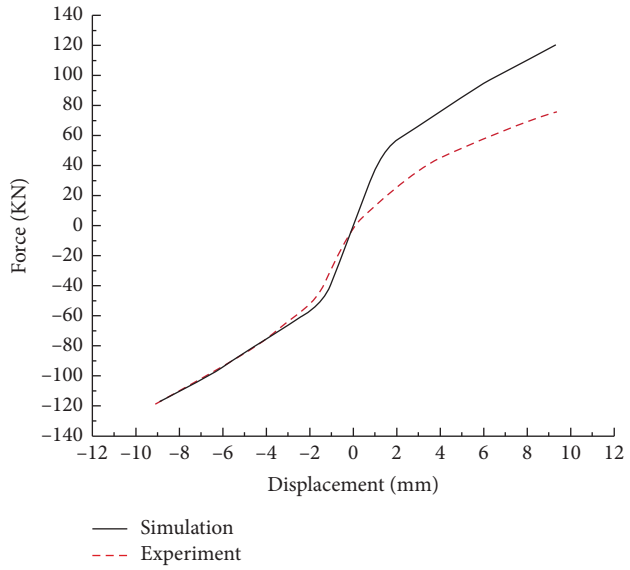

Figure 15: The skeleton curves of test and modelling results.

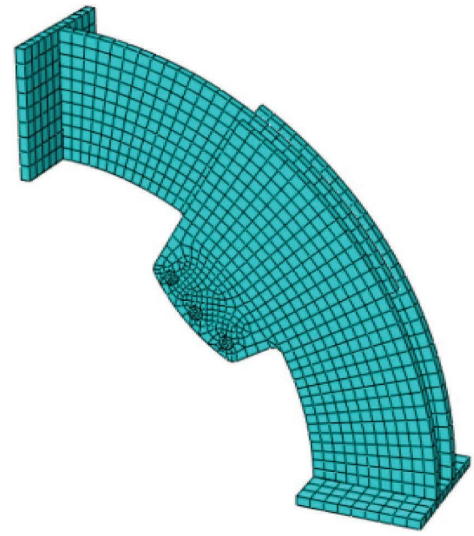

Figure 16: The mesh of LTLVNDs without amplification function.

4.3. Displacement Amplification Performance Analysis. To evaluate the displacement amplification performance of LTLVNDs, the amplification effect of LTLVNDs is studied by removing the amplification function part while keeping all other components unchanged. Figure 16 shows the FE model of the damper without amplification function. Figure 17 shows the hysteresis curve and the skeleton curve of LTLVNDs with and without amplification function. It can be observed that the energy dissipation capacity of the LTLVND equipped with amplification function is much better than that without amplification function. When the displacement is 4 mm, the hysteretic area of the former damper is 982 kN·mm, while that of the latter is 108 kN·mm, which means the amplification function part can significantly improve the energy dissipation capacity by 9 times compared to the damper without an amplification effect. A similar observation can be made for the initial stiffness of the damper.

4.4. Parametric Study. After validating the FE modelling procedure, the energy dissipation coefficient (ψ) and equivalent damping ratio (ξ), defined in equations (2) and (3), are used to evaluate damping performance. Note that the energy dissipation coefficient (ψ) reflecting the damper's energy dissipation capacity is the ratio of the energy dissipation to the maximum elastic potential energy in one period, and its value is as follows (Figure 18):

$$\psi = \frac{S_{(ABC+CDA)}}{S_{(OBE+ODF)}}. \quad (2)$$

The equivalent damping ratio (ξ) is defined in (3) to reflect the energy absorption capacity of the damper:

$$\xi = \frac{S_{(ABC+CDA)}}{4\pi S_{OBE}}. \quad (3)$$

A small-scale parametric study is then carried out to investigate the effect parameters including (i) the lead cylinder quantity (L) and (ii) the layout scheme of the lead cylinder (S) on the energy dissipation capacity of the LTLVND. Tables 2 and 3 list the analysis scenarios of the parametric study.

4.4.1. Quantity of Lead Cylinder (Q). It can be seen from Figure 19 that the enclosed area of the LTLVND hysteresis curve is directly proportional to the quantity of the lead cylinder (Q). For the cases with 30 mm diameter of the lead cylinder, when the applied displacement is 8 mm, the area formed by the hysteresis curve of P-4, P-5, and P-6 is equal to 605 kN·mm, 768 kNmm, and 982 kN·mm, respectively. This means that there is a 27% and 62% area increment for P-5 and P-6, respectively, compared with P-4. Hence, increasing the quantity of the lead cylinder (Q) can significantly enhance the energy dissipation capacity of the damper.

Table 4 lists the characteristic parameters including yielding force (F_y), initial stiffness (K_1), postyielding stiffness (K_2), equivalent damping ratio (ζ), and the energy dissipation coefficient (ψ) for different quantities of lead cylinders. As predicted, the yielding force (F_y) increases slightly as the number of lead cylinders increases. For example, F_y increases from 16.40 kN to 31.80 kN when Q increases from 1 to 3 for P-4, P-5, and P-6. A similar trend can be observed for initial stiffness (K_1). For the postyielding stiffness (K_2) of the damper, it is mainly determined by strain hardening of the lead cylinder and the shear stiffness of rubber. As that strain hardening of lead is very small, K_2 is significantly affected by rubber shear stiffness. K_2 increases by 20.7% from 16.50 kN/mm (P-4) to 19.92 kN/mm (P-6). The equivalent damping ratio (ξ) and the energy dissipation coefficient (ψ) also show the positive relationship with the quantity of the lead cylinder (Q).

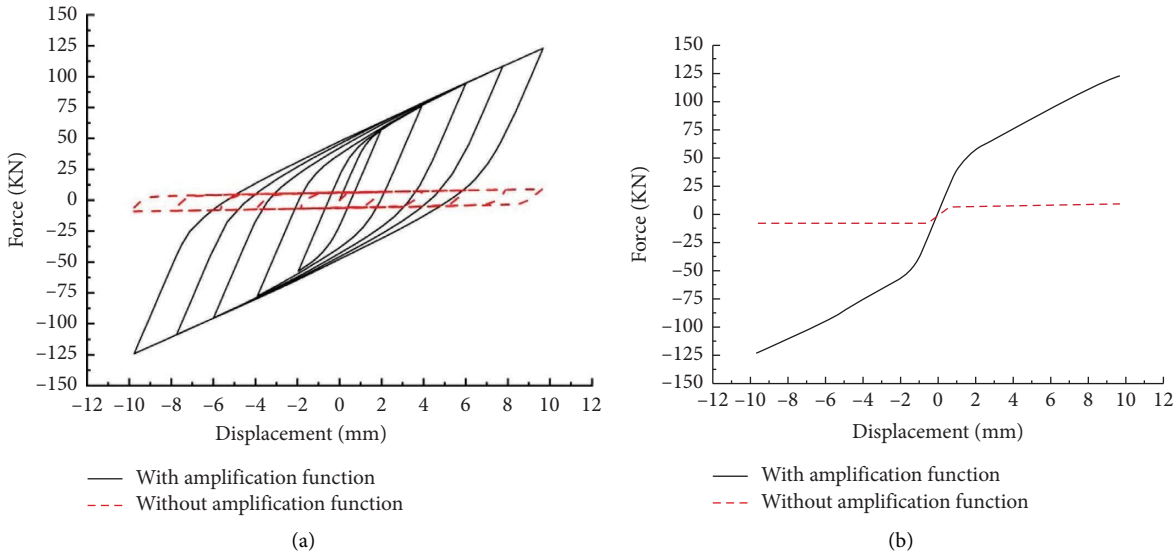

Figure 17: Comparison between LTLVND with and without amplification function. (a) Hysteresis curves. (b) Skeleton curves.

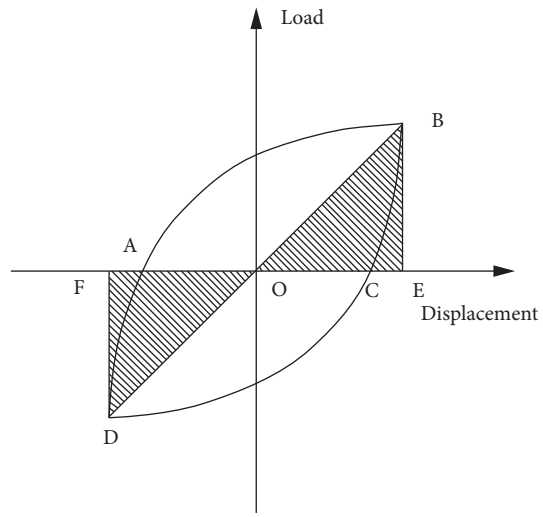

Figure 18: Calculation method of the energy dissipation coefficient and equivalent damping ratio.

Table 2: Parametric study of the quantity of the lead cylinder (Q).

Model label	Diameter of lead bar (D/mm)	Number of lead cylinders
P-1	20	1
P-2	20	2
P-3	20	3
P-4	30	1
P-5	30	2
P-6	30	3

Table 3: Parametric study of the layout scheme of the lead cylinder (L).

Model label	Scheme 1: (P-4)	Scheme 2: (P-7)	Scheme 3: (P-8)
Diameter of lead cylinder (D/mm)	30	21.4	17.4

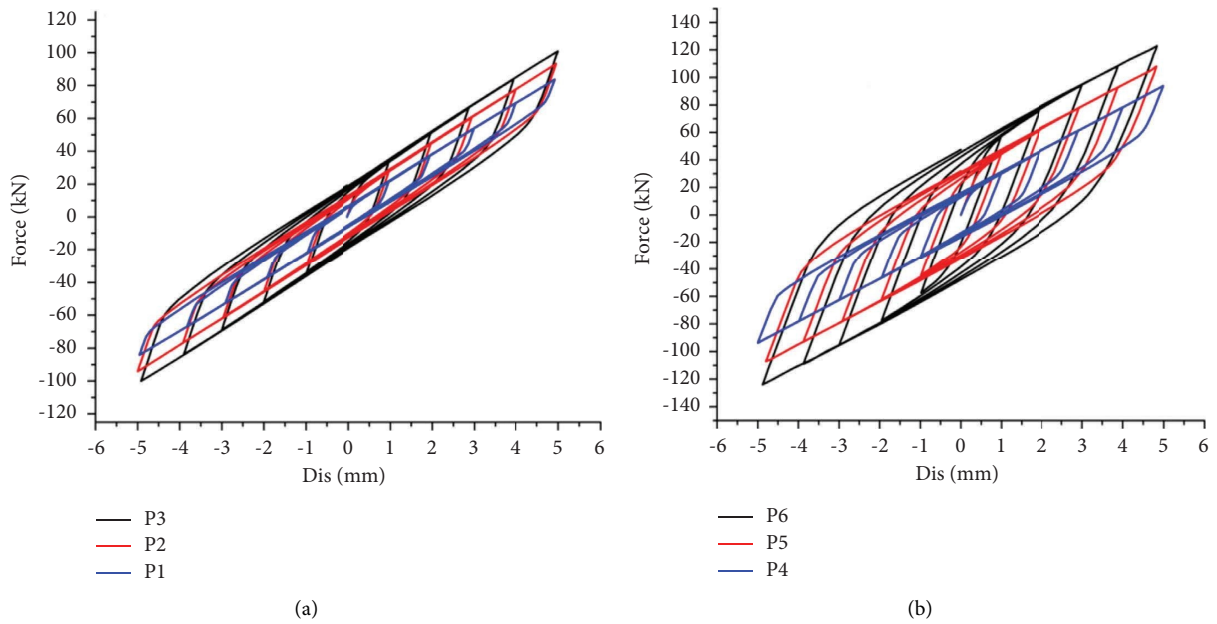

Figure 19: Hysteretic curves of different quantities of lead cylinders. (a) Lead cylinder with 20 mm diameter. (b) Lead cylinder with 30 mm diameter.

Table 4: Characteristic parameters of the dampers.

Model	F_y (kN)	K_1 (kN/mm)	K_2 (kN/mm)	ξ (%)	ψ
P-1	8.33	39.86	16.14	29.21	1.70
P-2	15.00	46.66	17.04	31.01	1.81
P-3	20.10	57.42	17.70	32.21	1.97
P-4	16.40	60.40	16.50	31.19	1.98
P-5	31.80	67.66	17.86	33.46	2.10
P-6	42.40	74.38	19.92	36.64	2.30

4.4.2. Layout Scheme of the Lead Cylinder (L). To study the impact of the layout scheme of the lead cylinder (L) at a given total area (S) of the cylinder, three layouts with different single-lead cylinder areas are considered (Table 3). Scheme 1 is the case of only one lead cylinder with a sectional area of S, Scheme 2 is the case of two lead cylinders each with a sectional area of 1/2 S, and Scheme 3 is the case of three lead cylinders each with a sectional area of 1/3 S.

As shown in Figure 20, the hysteresis curves of the three schemes are almost identical. However, a closer look reveals that Scheme 2 has slightly better energy dissipation capacity than the other two schemes at the yielding stage of reverse loading. Note that the area formed by the hysteresis curve of Scheme 1, Scheme 2, and Scheme 3 is equal to 605 kN·mm, 625 kN·mm, and 625 kN·mm, respectively. Hence, there is a 3.3% increase in energy dissipation capacity for Scheme 2.

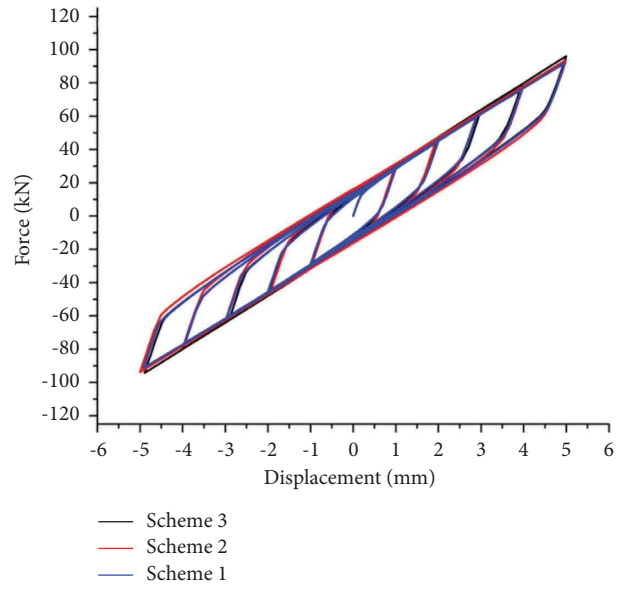

Figure 20: Comparison of hysteretic curves of the lead bar layout in different forms.

5. Seismic Analysis of Concrete Frame Structures with LTLVND

5.1. Constitutional Model of LTLVND. The constitutional model of LTLVNDs is first established before the seismic analysis of concrete frame structures with LTLVNDs. It is assumed that in the serviceability state, the lead cylinder is under an ideal elastic-plastic deformation mechanism and rubber remains a hyperelastic property. The mechanical behaviour of LTLVNDs can be described by a bilinear model consisting of initial stiffness K_1, postyielding stiffness K_2, yield force F_y, yield displacement U_Y, second stiffness reduction coefficient, and equivalent stiffness K_e. Figure 21 shows the bilinear mechanical model of LTLVNDs. Equations (4)–(6) give the definition of initial stiffness K_1, equivalent stiffness K_e, and α, respectively:

$$K_1 = \frac{F_y}{u_y}, \tag{4}$$

$$K_e = K_1\left(\frac{1-\alpha}{\mu} + \alpha\right), \tag{5}$$

$$\alpha = \frac{K_2}{K_1}. \tag{6}$$

Table 5 shows the characteristic parameters of the LTLVND's bilinear model with and without amplification function.

5.2. Building Model Overview. A six-story concrete frame model with a height of 4.2 m, a total transverse span of 504 m, and a longitudinal span of 252 m is created, as shown in Figure 22. Note that each of the transverse and longitudinal spans is 8.4 m. The structural layout is shown in Figures 23 and 24. The seismic design category is Category C, and the seismic intensity is VIII degrees according to the China Seismic Intensity Scale (CSIS), which means that the design base earthquake acceleration is 0.2 g. The soil category is Category II, the earthquake design group is Group II, and the structural safety level is Class II. The structure is designed to last 50 years. The floor dead load is 4 kN/m^2, the live load is 3 kN/m^2, and the basic wind pressure is 0.45 kN/m^2. The floor is 150 mm thick, and the beams are made of C40 concrete, while the columns are made of C60 concrete. The cross-sectional dimensions of the beams and columns are equal to 400×700 mm and 700×700 mm, respectively. Figure 22 shows the three-dimensional diagrams of the concrete frame structure.

5.3. Pushover Analysis of Concrete Frame Structures with LTLVND. The structural dampers should be given two directions (x-axis and y-axis in Figure 22) of the structure to suppress the torsional effect. In this study, three NLDV layout schemes are used to study the damping effect on the dynamics of structures under seismic excitation (Figures 25 and 26). Figure 27 shows the constitutive models of materials. Note that NLDVs are given on the side spans of the second and fourth floors for the y direction, while three different layout schemes are given for the x direction (Figures 25 and 26). The vibration mode analysis of the six-story concrete structure is first carried out to obtain the vibration period and mode of the structure. In order to compare the analysis result of the vibration mode analysis, two FE modelling and visualization tools for the structural analysis and design of buildings, i.e., ETABS and PKPM, are used to analyse the vibration period and mode of the undamped frame structure. Table 6 shows the analysis results. It can be seen that the primary vibration mode from ETABS and PKPM is the same and that the period error is within 10%.

The pushover analysis is then carried out for the six-story frame structure under different damper arrangement schemes. The uniform load and the inverted triangle load are used. The pushover curves of each model in the two loading scenarios are as shown in Figure 28. It can be seen that overall structural rigidity and load-bearing capacity have increased significantly when NLDV dampers are equipped. The structural rigidity and load-bearing capacity of Scheme III are slightly higher than those of Schemes I and II. Therefore, it is concluded that Scheme III and the number of dampers have a greater impact on the energy consumption effect.

The shear forces for the performance point of the six-story concrete frame structure with LTLVNDs installed are shown in Table 7. It can be seen that the structure equipped with LTLVNDs has a smaller shear force and displacement at the performance point than that of the original concrete frame structure. The mitigation effect of LTLVND-1 is better than that of LTLVND-2. Figure 29 shows story drift for the six-story frame structure under different damper arrangement schemes. As predicted, the structure with dampers has a significant reduction in story drift for high levels. Scheme III for LTLVND-1 can produce the minimum story drift among all cases, with a 25% reduction for the top floor under uniform loads compared to the structure without dampers. Under an inverted triangle load, it can achieve a 27.2% reduction in story drift at the top floor. In addition, LTLVND-1 has a more effective mitigation effect than LTLVND-2.

Figure 30 shows a comparison of the interstory drift angle under different damper arrangement schemes. For both the uniform and inverted triangle load cases, the structure with dampers has smaller interstory drift angles than the original concrete structure. The second floor has the largest interstory drift angle, indicating that it is the weakest in terms of structural stiffness. Similar to story drift, Scheme III of LTLVND-1 can produce the minimum interstory drift angle among all cases where a 25% reduction can be achieved for the second floor under uniform loading compared to the structure without dampers.

5.4. Dynamic Elastoplastic Analysis. Dynamic elastoplastic analysis can specify the dynamic response of the structure and can verify the accuracy of the pushover analysis. It is therefore one of the popular ways to evaluate the seismic performance of structures. The dynamic characteristics of the structure under three seismic waves are studied for the seismic mitigation effect of NLDV-1 and NLDV-2 dampers. At present, there are two popular ways to obtain seismic waves. One is the artificial wave generated according to the design codes, and the other one is to integrate several selected waves from the existing wave library. Figure 31 shows the three selected seismic waves, including two natural waves and one artificial wave, input to the structure along the x direction.

Figures 32–34 show the displacement curves at the top floor of the six-story frame structure for different damper arrangements. It can be observed that that NLDV-1 has a better mitigation effect than LTLVND-2 for the three selected waves. Scheme III produces the smallest displacement of the top floor for different damper arrangement

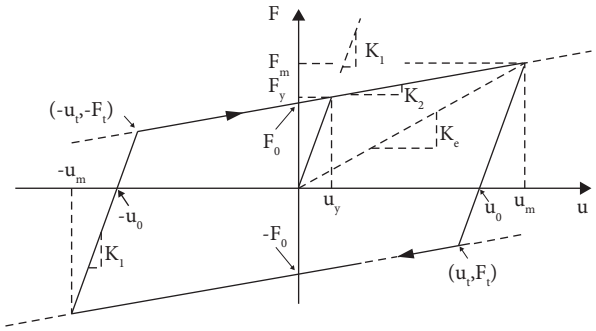

Figure 21: Bilinear constitutional model.

Table 5: Comparison of the characteristic parameters of LTLVNDs with and without amplification function.

Damper types	Characteristic parameters of dampers			
	Yield strength (kN)	Initial stiffness (kN/mm)	Equivalent stiffness (kN/mm)	Postyield ratio
LTLVND (with amplification function)	56.417	80.595	12.703	0.300
LTLVND (without amplification function)	6.517	21.723	1.500	0.025

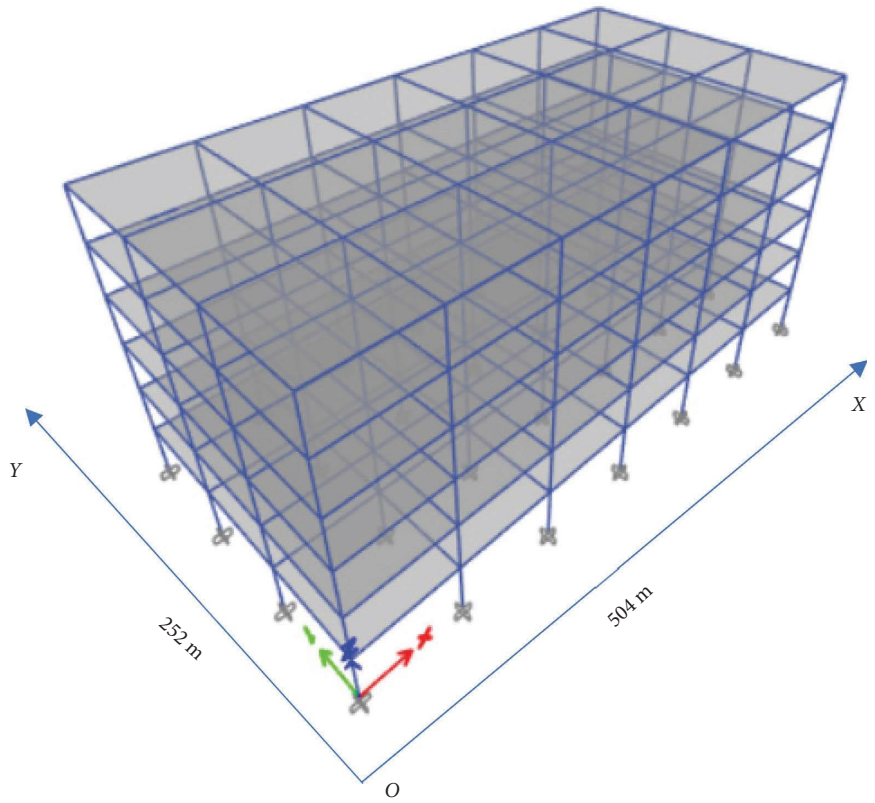

Figure 22: A concrete frame model with six stories.

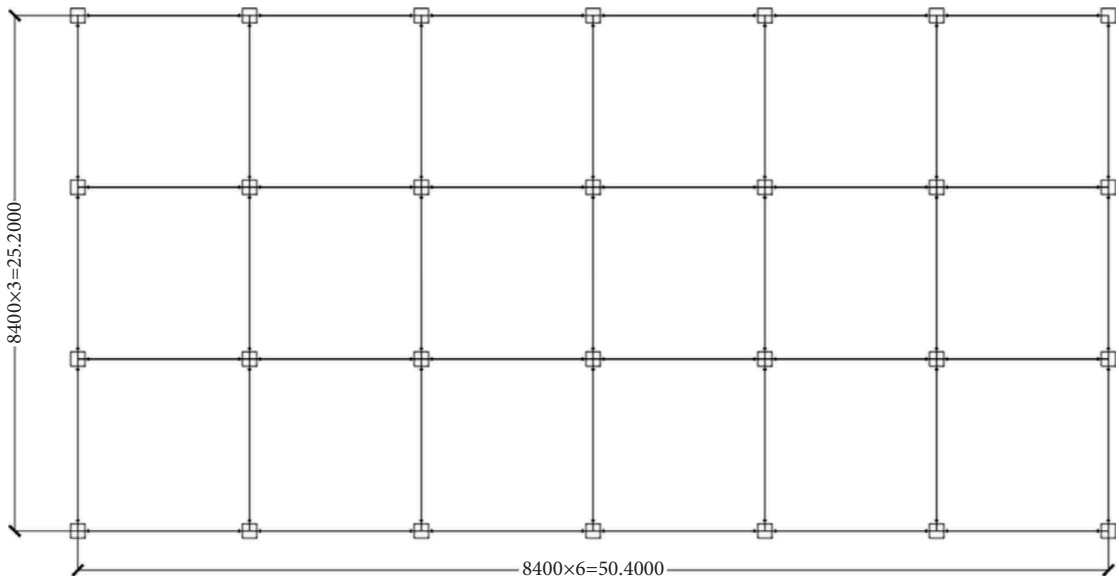

Figure 23: Top view of the concrete frame model.

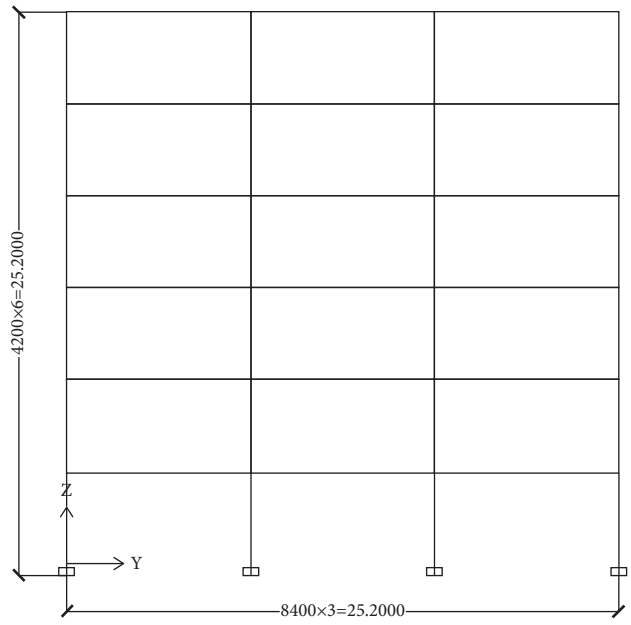

Figure 24: Side view of the concrete frame model.

schemes. The mitigation effect of the dampers is quite obvious as the maximum accelerations of the structure with dampers are significantly lower than those of the original structure. Scheme III can produce the best acceleration reduction effect. The maximum displacement is 208 mm in wave 1, and the minimum displacement is 114 mm in the structure with LTLVND-1 under the Scheme III arrangement, which can produce a 38% reduction for the maximum amplitude.

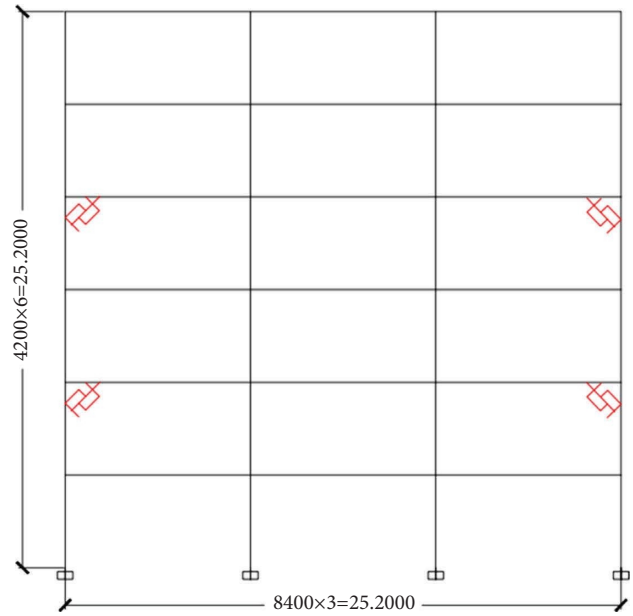

Figure 25: Side view of the damper's arrangement.

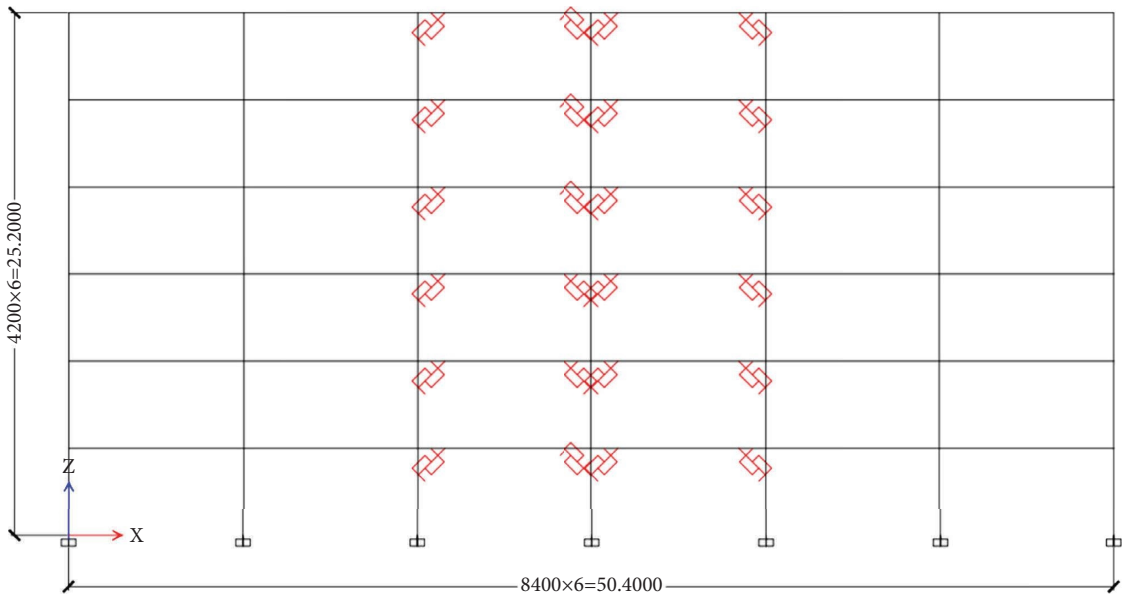

(a)

Figure 26: Continued.

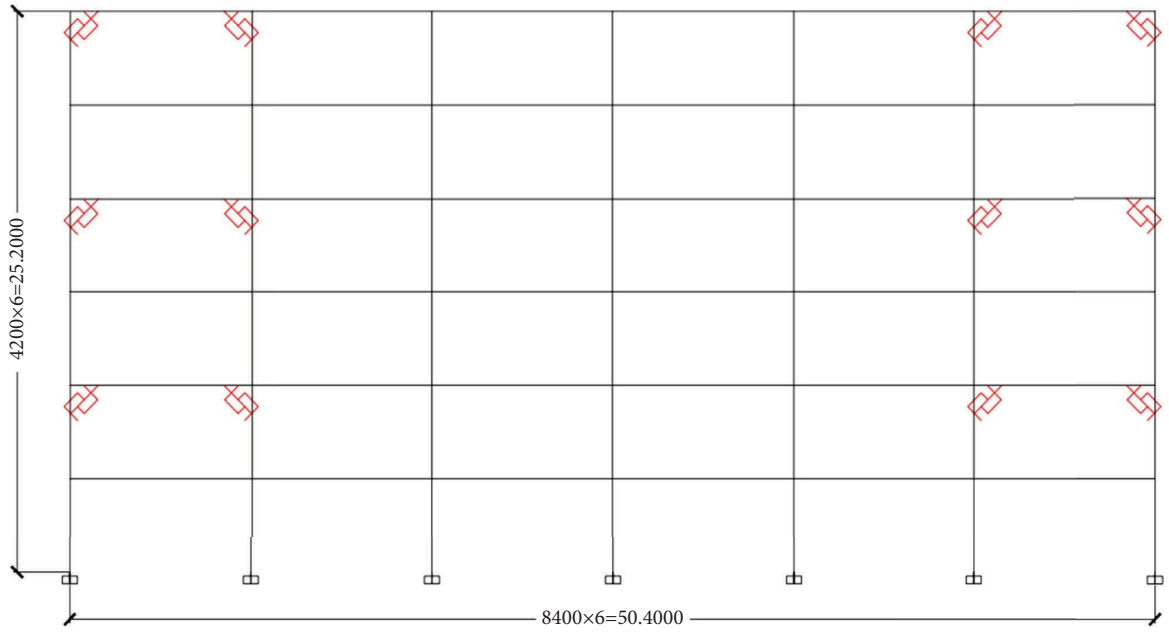

(b)

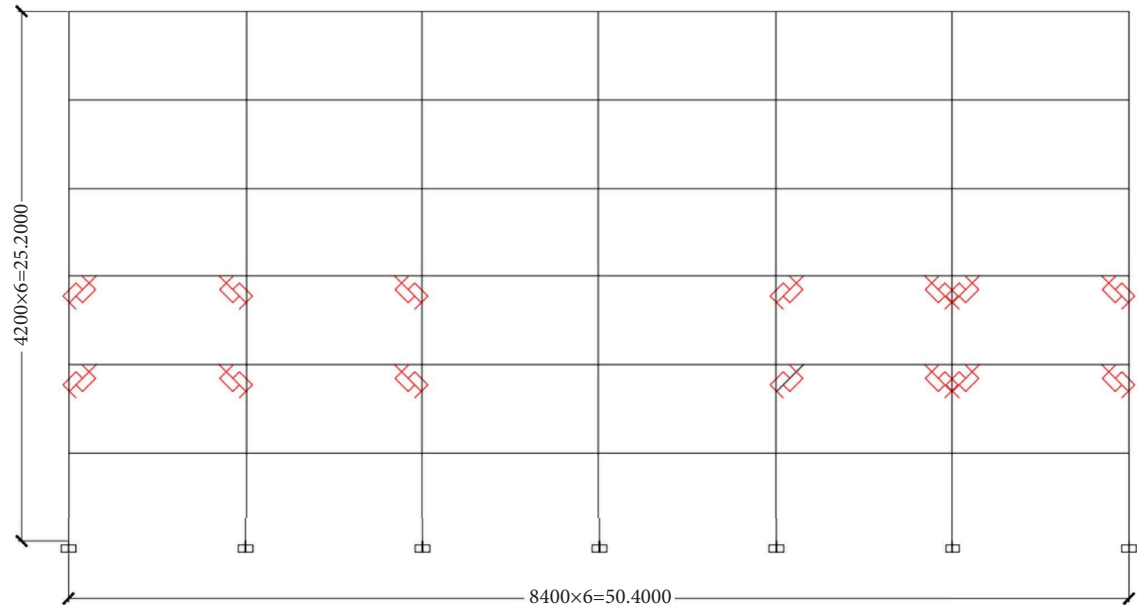

(c)

Figure 26: Three ILDV layout schemes. (a) Scheme I. (b) Scheme II. (c) Scheme III.

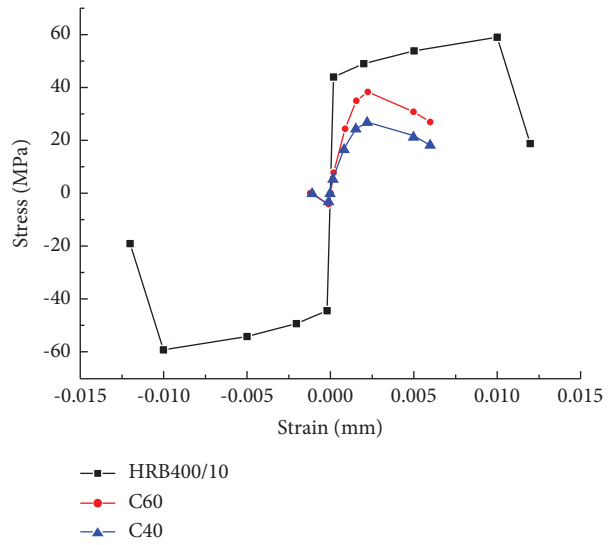

Figure 27: The constitutive models of the materials.

Table 6: The vibration period and mode of the undamped frame structure.

	PKPM	ETABS	Error (%)	Vibration mode
T1	1.109	1.058	4.5	First-order translation along y
T2	1.086	1.019	6.2	First-order translation along x
T3	0.992	0.952	4.0	First-order rotation along z
T4	0.372	0.337	9.4	Second-order translation along y
T5	0.343	0.326	5.0	Second-order translation along x

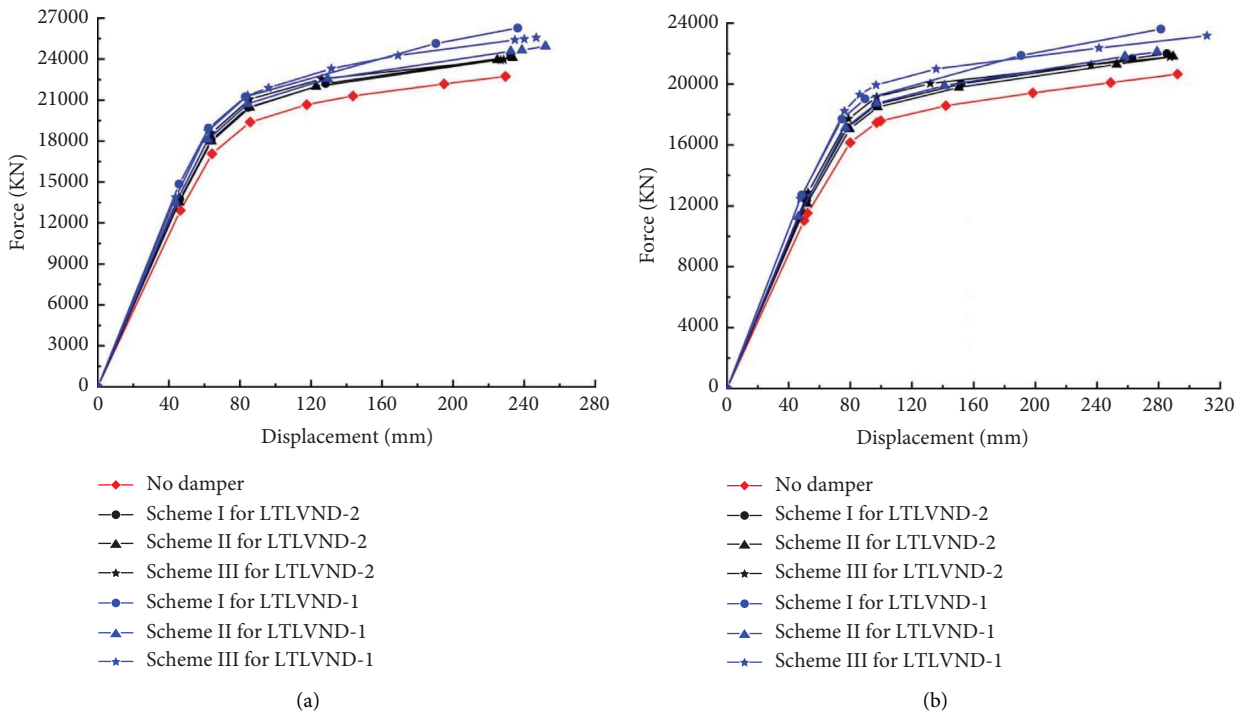

Figure 28: The pushover analysis results. (a) Pushover analysis curves under a uniform load. (b) Pushover analysis curves under an inverted triangle load.

Table 7: The shear force for the performance point of the six-story concrete frame structure.

No	Case	Maximum shear force (kN)			
		Uniform load	Amplitude gain (%)	Inverted triangle load	Amplitude gain (%)
1	No damper	22293	0.0	20655	0.0
2	Scheme I for LTLVND-2	24176	8.4	22000	6.5
	Scheme I for LTLVND-1	26270	17.8	23608	14.2
3	Scheme II for LTLVND-2	24090	8.1	21818	5.6
	Scheme II for LTLVND-1	24945	11.9	22119	7.1
4	Scheme III for LTLVND-2	23959	7.8	21784	5.5
	Scheme III for LTLVND-1	25573	14.7	23178	12.2

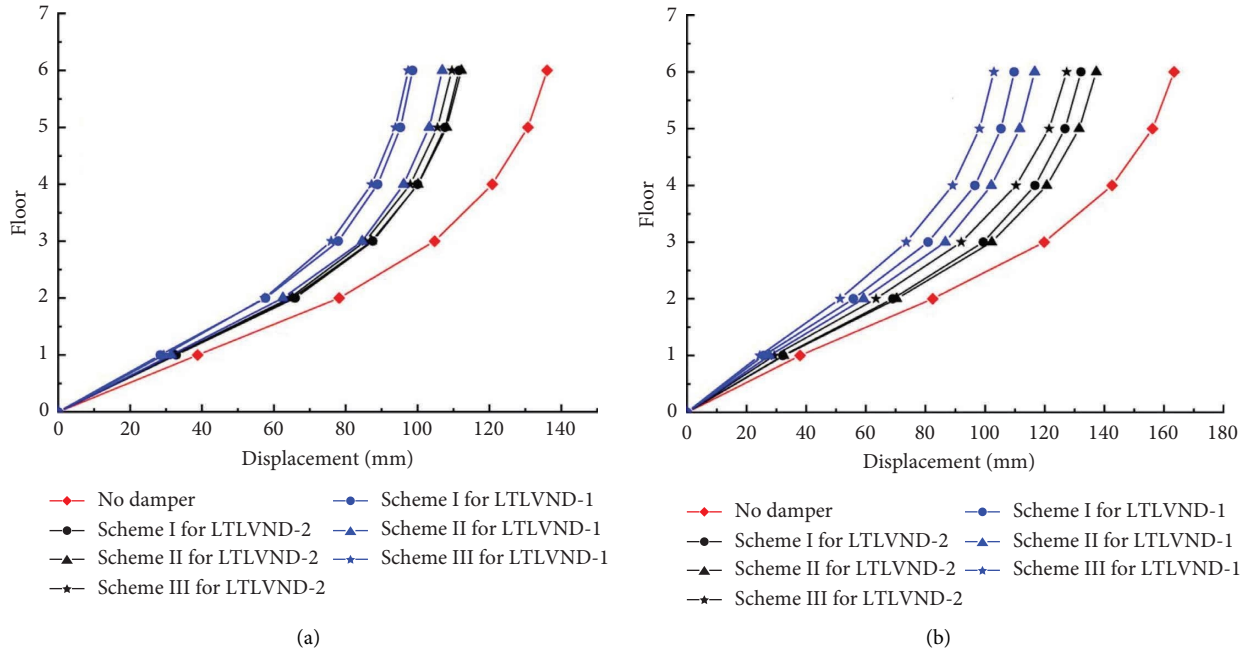

Figure 29: The story drift analysis. (a) Story drift curves under a uniform load. (b) Story drift curves under an inverted triangle load.

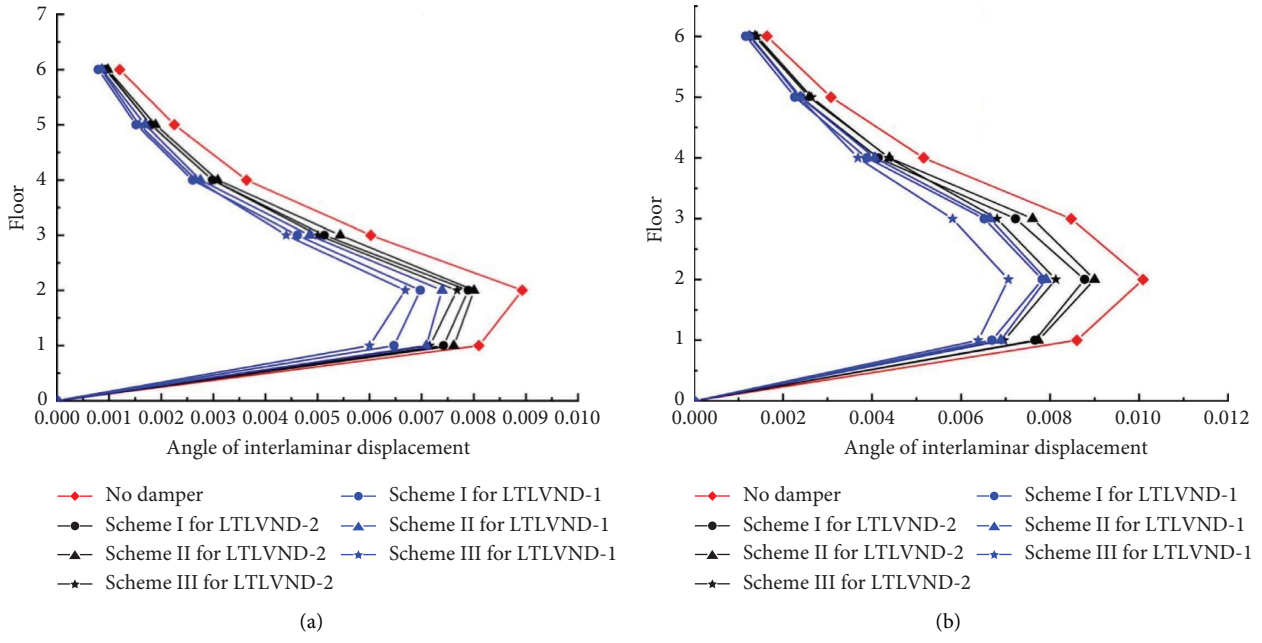

Figure 30: The interstory drift angle analysis. (a) Interstory drift angle curves under a uniform load. (b) Interstory drift angle curves under an inverted triangle load.

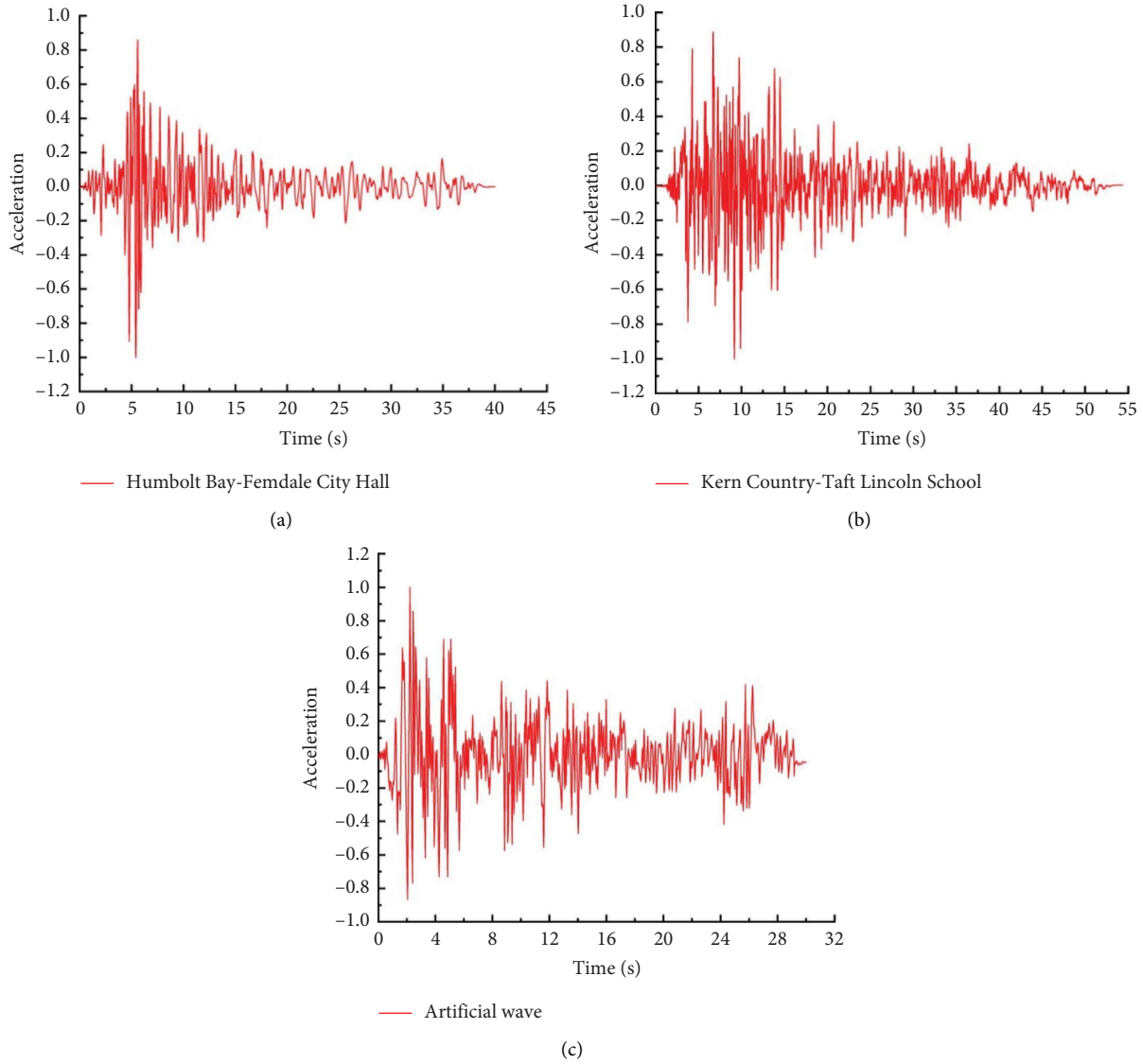

Figure 31: Three selected seismic waves. (a) Wave 1 for dynamic analysis. (b) Wave 2 for dynamic analysis. (c) Wave 3 for dynamic analysis.

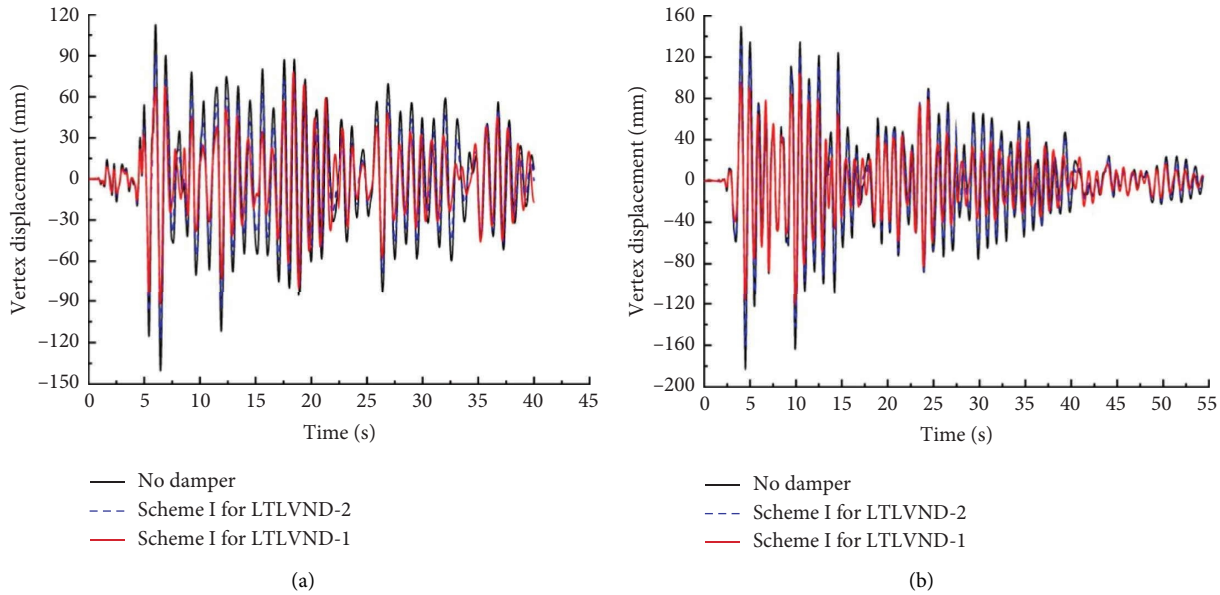

Figure 32: Continued.

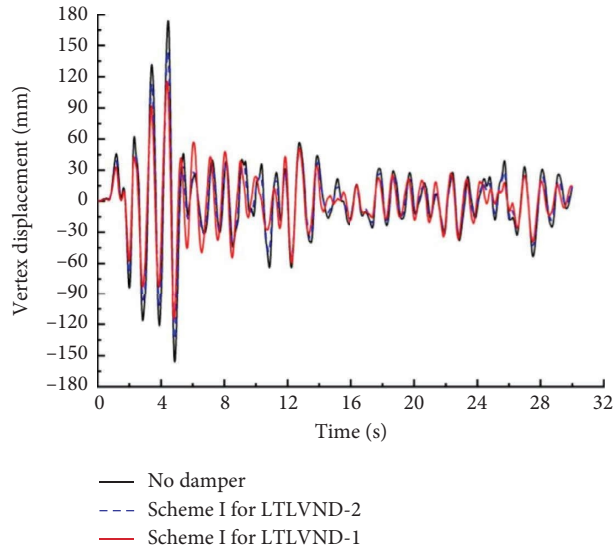

(c)

FIGURE 32: The displacement curves at the top floor of the six-story frame structure for Scheme 1. (a) Displacement curves under wave 1 input. (b) Displacement curves under wave 2 input. (c) Displacement curves under wave 3 input.

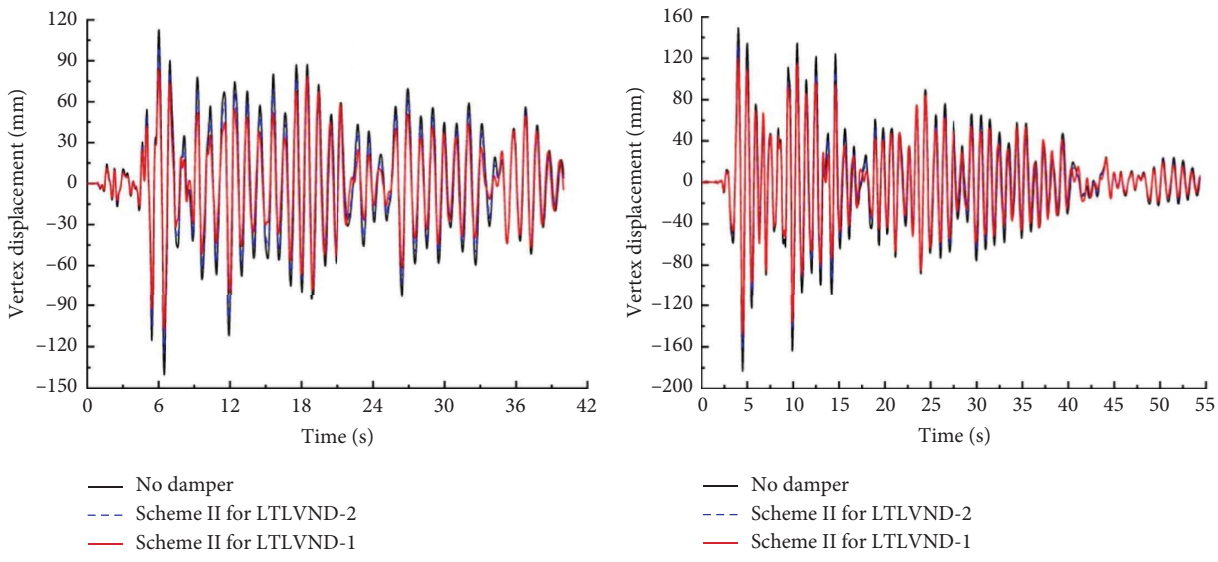

(a) (b)

FIGURE 33: Continued.

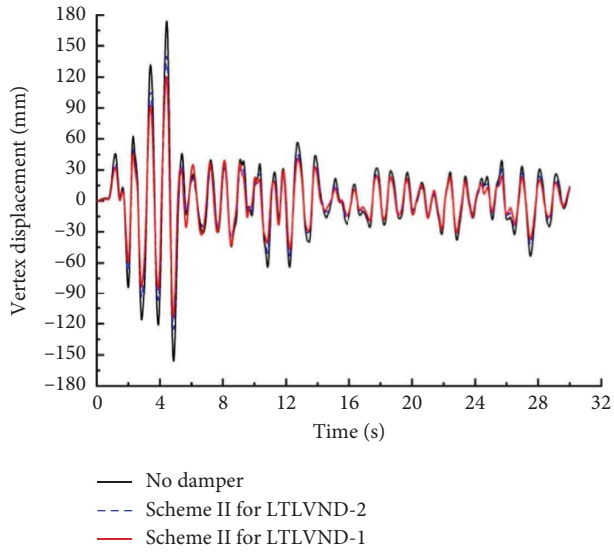

(c)

Figure 33: The displacement curves at the top floor of the six-story frame structure for Scheme 2. (a) Displacement curves under wave 1 input. (b) Displacement curves under wave 2 input. (c) Displacement curves under wave 3 input.

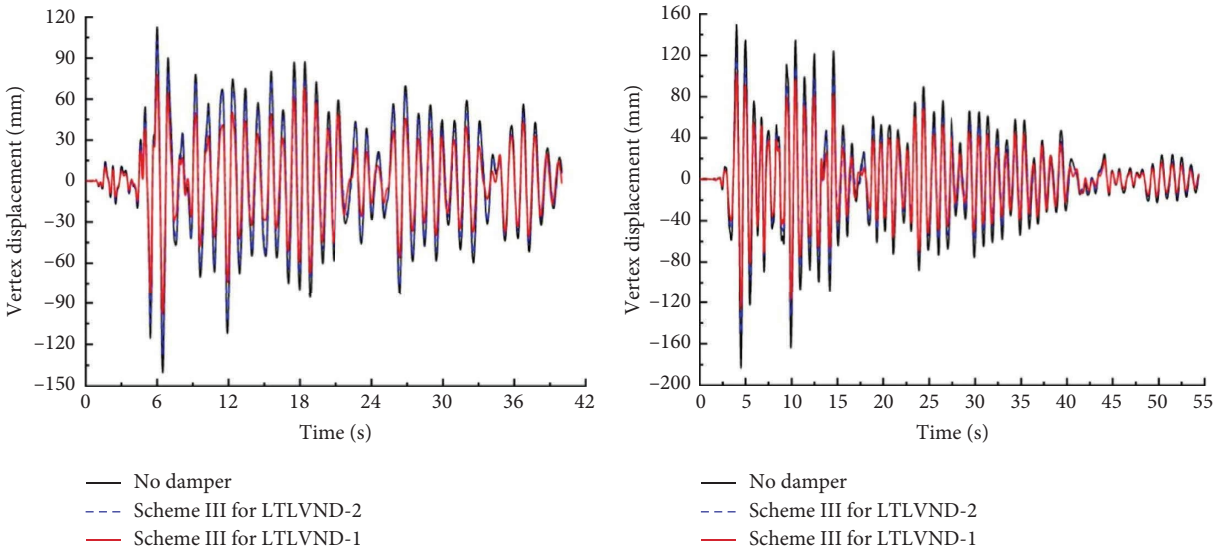

(a) (b)

Figure 34: Continued.

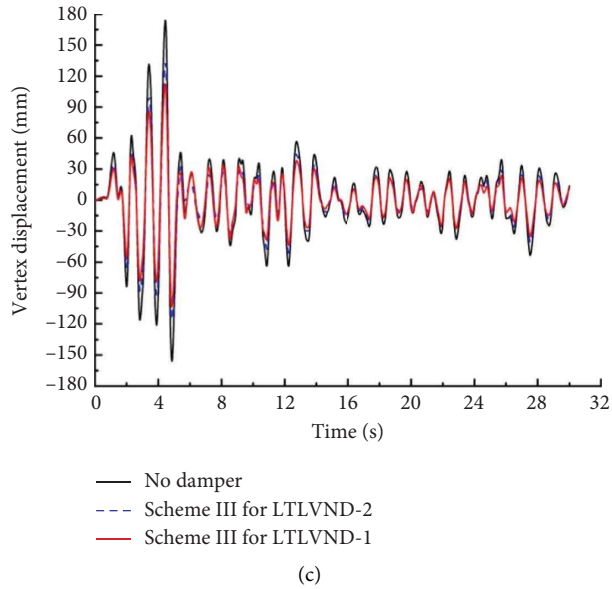

(c)

Figure 34: The displacement curves at the top floor of the six-story frame structure for Scheme 3. (a) Displacement curves under wave 1 input. (b) Displacement curves under wave 2 input. (c) Displacement curves under wave 3 input.

6. Conclusions

In this study, an innovative lead viscoelastic damper (LTLVND) is proposed that can capture small rotational displacements of the infrastructure under seismic excitation based on the leverage effect. The characteristics of energy-absorbing capacities of the LTLVND and its mitigation effect on the dynamics of structures under seismic excitation are studied. The test results show that a satisfactory energy dissipation effect can be observed for the innovative lead viscoelastic damper (LTLVND). The hysteresis curve of the damper shows a parallelogram shape, and the hysteresis envelope is reasonably good, so that strong energy dissipation capacity is obtained without material yielding. Finally, a small-scale FE parametric study is organized to investigate the effect of geometrical parameters of the damper model on the energy dissipation capacity with the conclusion that with the increase in the number of lead cylinders, the energy dissipation capacity increases.

Data Availability

Some or all data, models, or code that support the findings of this study are available from the corresponding author upon reasonable request.

Disclosure

Any opinions, findings, and conclusions expressed in this paper are those solely of the authors and do not necessarily reflect the view of Guangzhou University. The authorship arrangement has been reviewed and approved by Guangzhou University in accordance with its policy on objectivity in research.

Conflicts of Interest

The authors declare that they have no conflicts of interest.

Acknowledgments

The author of this paper receives research funding from the National Science Fund for Distinguished Young Scholars (51925802), 100 Innovative Leading Talents Plan of Guangzhou, STU Scientific Research Foundation for Talents (NTF22010), Science and Technology Projects in Guangzhou (202102010482 and SL2022A03J00954), and Natural Science Foundation Funding of Guangdong Province (Nos. 2023A1515012502 and 2018A030310070).

References

[1] F. Taiyari, F. M. Mazzolani, and S. Bagheri, "Damage-based optimal design of friction dampers in multistory chevron braced steel frames," *Soil Dynamics and Earthquake Engineering*, vol. 119, pp. 11–20, 2019.

[2] I. H. Mualla and B. Belev, "Performance of steel frames with a new friction damper device under earthquake excitation," *Engineering Structures*, vol. 24, no. 3, pp. 365–371, 2002.

[3] S. H. Lee, J. H. Park, S. K. Lee, and K. W. Min, "Allocation and slip load of friction dampers for a seismically excited building structure based on storey shear force distribution," *Engineering Structures*, vol. 30, no. 4, pp. 930–940, 2008.

[4] H. S. Monir and K. Zeynali, "A modified friction damper for diagonal bracing of structures," *Journal of Constructional Steel Research*, vol. 87, pp. 17–30, 2013.

[5] R. I. Skinner, J. M. Kelly, and A. J. Heine, "Hysteretic dampers for earthquake-resistant structures," *Earthquake Engineering & Structural Dynamics*, vol. 3, no. 3, pp. 287–296, 1974.

[6] K. C. Tsai, H. W. Chen, C. P. Hong, and Y. F. Su, "Design of steel triangular plate energy absorbers for seismic resistant construction," *Earthquake Spectra*, vol. 9, no. 3, pp. 505–528, 1993.

[7] B. Morgen and Y. Kurama, "A friction damper for post-tensioned precast concrete moment frames," *PCI Journal*, vol. 49, no. 4, pp. 112–133, 2004.

[8] T. Rossetto and A. Elnashai, "Derivation of vulnerability functions for European-type RC structures based on observational data," *Engineering Structures*, vol. 25, no. 10, pp. 1241–1263, 2003.

[9] T. Roy and V. Matsagar, "Effectiveness of passive response control devices in buildings under earthquake and wind during design life," *Structure and Infrastructure Engineering*, vol. 15, no. 2, pp. 252–268, 2019.

[10] D. R. Pant, M. Montgomery, and C. Christopoulos, "Full-scale testing of a viscoelastic coupling damper for high-rise building applications and comparative evaluation of different numerical models," *Journal of Structural Engineering*, vol. 145, no. 2, 2019.

[11] M. Rahimiasl and A. Bakhshi, "The effects of viscous dampers on the reliability of steel structures using a PIF index," *Proceedings of the Institution of Civil Engineers- Structures and Buildings*, vol. 172, no. 4, pp. 289–300, 2019.

[12] K. Kinali and B. R. Ellingwood, "Seismic fragility assessment of steel frames for consequence-based engineering: a case study for Memphis, TN," *Engineering Structures*, vol. 29, no. 6, pp. 1115–1127, 2007.

[13] D. G. Lignos and E. Karamanci, "Drift-based and dual-parameter fragility curves for concentrically braced frames in seismic regions," *Journal of Constructional Steel Research*, vol. 90, pp. 209–220, 2013.

[14] E. Choi, G. Choi, H.-T. Kim, and H. Youn, "Smart damper using the combination of magnetic friction and pre-compressed rubber springs," *Journal of Sound and Vibration*, vol. 351, pp. 68–89, 2015.

[15] E. Gandelli, A. Taras, J. Distl, and V. Quaglini, "Means of hysteretic braces: influence on acceleration-sensitive non-stuctureal components," *Frontiers in Building Environment*, vol. 5, pp. 1–13, 2019.

[16] J. Iyama, C. Y. Seo, J. M. Ricles, and R. Sause, "Self-centering MRFs with bottom flange friction devices under earthquake loading," *Journal of Constructional Steel Research*, vol. 65, no. 2, pp. 314–325, 2009.

[17] P. Rojas, J. M. Ricles, and R. Sause, "Seismic performance of post-tensioned steel moment resisting frames with friction devices," *Journal of Structural Engineering*, vol. 131, no. 4, pp. 529–540, 2005.

[18] B. G. Morgen and Y. C. Kurama, "Characterization of two friction interfaces for use in seismic damper applications," *Materials and Structures*, vol. 42, no. 1, pp. 35–49, 2009.

[19] M. N. Eldin, A. J. Dereje, and J. Kim, "Seismic retrofit of rc buildings using self-centring pc frames with friction-dampers," *Engineering Structures*, vol. 208, pp. 10–25, 2020.

[20] B. Wang, S. Zhu, K. Chen, and J. Huang, "Development of superelastic SMA angles as seismic-resistant self-centering devices," *Engineering Structures*, vol. 218, Article ID 110836, 2020.

[21] S. Dehghani, S. F. Fathizadeh, T. Y. Yang et al., "Performance evaluation of curved damper truss moment frames designed using equivalent energy design procedure," *Engineering Structures*, vol. 226, Article ID 111363, 2021.

[22] C. Fang, W. Wang, and W. Feng, "Experimental and numerical studies on self-centring beam-to-column connections free from frame expansion," *Engineering Structures*, vol. 198, Article ID 109526, 2019.

[23] Y.-R. Dong, Z.-D. Xu, Q.-Q. Li, Y. S. Xu, and Z. H. Chen, "Seismic behavior and damage evolution for retrofitted RC frames using haunch viscoelastic damping braces," *Engineering Structures*, vol. 199, Article ID 109583, 2019.

[24] M. Constantinou, P. Tsopelas, W. Hammel, and A. N. Sigaher, "Toggle-brace-damper seismic energy dissipation systems," *Journal of Structural Engineering*, vol. 127, no. 2, pp. 105–112, 2001.

[25] A. Sigaher and M. Constantinou, "Scissor-jack-damper energy dissipation system," *Earthquake Spectra*, vol. 19, no. 1, pp. 133–158, 2003.

[26] J. S. Hwang, J. Kim, and Y. M. Kim, "Rotational inertia dampers with toggle bracing for vibration control of a building structure," *Engineering Structures*, vol. 29, no. 6, pp. 1201–1208, 2007.

[27] S. Berton and J. E. Bolander, "Amplification system for supple-mental damping devices in seismic applications," *Journal of Structural Engineering*, vol. 131, no. 6, pp. 979–983, 2005.

[28] Y. Ribakov and A. M. Reinhorn, "Design of amplified structural damping using optimal considerations," *Journal of Structural Engineering*, vol. 129, no. 10, pp. 1422–1427, 2003.

[29] A. Zasso, A. M. Aly, and F. Resta, "MR dampers with lever mechanism for response reduction in high-rise buildings under wind loads," in *Proceedings of the 5th European & African Conference on Wind Engineering*, Firenze University Press, Florence, Italy, July 2009.

[30] H. Hsu and H. Halim, "Brace Performance with steel curved dampers and amplified deformation mechanisms," *Engineering Structures*, vol. 175, no. 8, pp. 628–644, 2018.

[31] J. S. B. Mosquera, J. L. Almazán, and N. F. Tapia, "Amplification system for concentrated and distributed energy dissipation devices," *Earthquake Engineering & Structural Dynamics*, vol. 45, no. 6, pp. 935–956, 2016.

[32] Z. Zhang, K. Bi, H. Hao, P. Sheng, L. Feng, and D. Xiao, "Development of a novel deformation-amplified shape memory alloy-friction damper for mitigating seismic responses of RC frame buildings," *Engineering Structures*, vol. 216, no. 63, pp. 110751–111139, 2020.

[33] M. Leblouba, A. Fageeri, and Z. A. Al-Sadoon, "A novel seismic energy dissipation device: laboratory tests, mathematical modeling, and numerical analysis," *Soil Dynamics and Earthquake Engineering*, vol. 162, 2022.

[34] L. L. Song, T. Guo, and C. Chen, "Experimental and numerical study of a self-centering prestressed concrete moment resisting frame connection with bolted web friction devices," *Earthquake Engineering & Structural Dynamics*, vol. 43, no. 4, pp. 529–545, 2014.

[35] K. Lin, X. Lu, Y. Li, and H. Guan, "Experimental study of a novel multi-hazard resistant prefabricated concrete frame structure," *Soil Dynamics and Earthquake Engineering*, vol. 119, pp. 390–407, 2019.

[36] Y. R. Dong, Z. D. Xu, Q. Q. Li, Y.-S. Xu, and Z.-H. Chen, "Seismic behavior and damage evolution for retrofitted RC frames using haunch viscoelastic damping braces," *Engineering Structures*, vol. 199, pp. 1–13, 2019.

[37] Hibbitt, Karlsson, and Sorensen, *ABAQUS User Manual, Version 6.14*, Hobbit, Karlsson & Sorensen Inc, Providence, RI, USA, 2014.